Advanced Nonlinear Controller of Single Phase Shunt Active Power Filter Interfacing Solar Photovoltaic Source and Electrical Power Grid

Zineb Hekss[a,*], Abdelmajid Abouloifa[a], Ibtissam Lachkar[b], Abdelali El Aroudi[c], Salwa Echalih[a] and Fouad Giri[d]

[a]TI Lab, Faculty of Sciences Ben M'sick, Hassan II University, BP 7955 Casablanca, Morocco
[b]ESE lab, ENSEM of Casablanca, Hassan II University, BP 8118 Casablanca, Morocco
[c]Department d'Enginyeria Electrònica, Elèctrica i Automàtica, Universitat Rovira i Virgili, 43003 Tarragona, Spain
[d]Normandie UNIV, UNICAEN, ENSICAEN, LAC, 14000 Caen, France

ARTICLE INFO

Keywords:
Solar Photovoltaic system
Shunt active power filter
Nonlinear control
Average analysis
Lyapunov stability analysis
Power factor correction

ABSTRACT

This paper addresses the nonlinear controller design and the stability analysis of a shunt active power filter (SAPF) interfacing a solar photovoltaic (PV) system which consists of a couple PV panels, a single-phase two-stage IGBT half-bridge SAPF and two identical DC link capacitors. We seek for the considered system the fulfillment of three control objectives: (i) extracting the maximum PV power using an appropriate maximum power point tracking (MPPT) algorithm; (ii) regulation of the DC link capacitor voltages to the reference provided by the MPPT controller hence ensuring the exchange of power between the PV source and the AC power grid; (iii) compensation for reactive power and undesired harmonic caused by the nonlinearity of electronic power loads, i.e.performing power factor correction (PFC). The control objectives are achieved using a new two-loop cascaded controller. The Backstepping approach is applied in the inner loop to perform PFC. A filtered proportional-integral (PI) controller is applied in the outer loop to ensure tight regulation of the PV voltage. The MPPT control is implemented using a perturb-and-observe (PO) algorithm. The performance of the closed loop system under the two-loop control strategy is formally analyzed through the Lyapunov approach applied to the averaged model. Numerical simulations are performed in MATLAB/SimPowerSystems environment to validate the design methodology and to confirm the theoretically predicted performances of the system under the proposed nonlinear controller.

1. Introduction

The penetration of power electronic devices in electrical power grids have grown considerably in recent years. In this regard, it is well known that these devices act as nonlinear loads for the power grid and have become major causes of the degradation of power quality because of its strongly nonlinear nature [2, 7] leading them to modify the sinusoidal shape of the alternating current by injecting undesired higher order harmonics and reactive power into the electrical power system. This results in many adverse effects such as excessive equipment overheating, excessive transmission power losses, low system efficiency and deterioration of power factor [19, 26]. An effective way to mitigate these problems in this kind of applications is by using shunt active power filters (SAPFs) known by their good filtering capacity and flexibility [29]. Indeed, SAPF interactive PV systems are widely used as a better choice and are designed to operate in parallel with nonlinear loads for transferring the active power and compensating the undesired harmonics and reactive power simultaneously.

SAPF-PV systems are usually classified according to their operational applications and to the way they are connected to power sources and electronic loads. In this regard, two principal topologies can be distinguished. In the first one a DC-DC converter is used for tracking maximum power from solar PV panels and an SAPF is used to improve power quality [26, 31]. In the second one, the PV source is connected to the power grid via an SAPF to ensure the MPPT functionality and the power quality requirement by compensating for harmonic currents and reactive power

*Corresponding author
zineb.hekss-etu@etu.univh2c.ma (Z. Hekss)
ORCID(s): 0000-0003-0494-1070 (Z. Hekss)

[17, 18]. Among the more usual MPPT algorithms are the perturb-and-observe (PO) algorithm and incremental conductance (IC) algorithm [16, 4]. The single phase SAPF has attracted the attention of many researchers because of its simple design and low cost [17, 18, 3, 8, 9, 22]. In a three phase system, the SAPF can be inserted at each phase of the nonlinear load and this way proves to be much suitable than implementing a higher power three phase SAPF [29, 1, 27]. The half bridge SAPF topology offers interesting practical benefits compared to the conventional full-bridge converter. For instance, it allows the reduction of the switching losses of the given power semiconductors thus increasing the reliability of the system [17, 18, 6].

Various control strategies have been proposed for SAPF over the last decade. An extensive review about harmonic mitigation can be found in [19]. A fuzzy predictive direct power control of a three-phase SAPF-PV system is discussed in [28]. An adaptive linear neural network approach of single phase SAPF-PV is proposed in [26]. Another important approach was discussed in [24] where the authors proposed an indirect current control for single-phase SAPF showing that the indirect control approach features a higher speed and lower control functions since no current harmonic detection method is needed as compared to the direct control approach. An adaptive backstepping fuzzy neural controller based on fuzzy sliding mode control was discussed in [11] for a three-phase SAPF. An adaptive backstepping control of single phase SAPF is designed in [30]. In [22], a Lyapunov control design based on linearized model of single phase SAPF was discussed. In the same vein, a new approach for three phase SAPF, using a feedback-linearization approach was proposed in [23]. Linearization-based methods have certain limitations and are only effective when the system operating point remains in the proximity of the point for which the controller is designed. The use of the nonlinear averaged model in control design provides more consistent control activity guaranteeing global convergence of the system to the desired operating point and better protection for actuators [15, 21, 25, 5]. A Lyapunov design approach with an adaptive observer has been well discussed in [1] for three phase SAPF to achieve PFC, without assuming the grid power characteristics to be a priori known. In the same vein, a Lyapunov technique with Kalman observer of single phase SAPF is discussed in [3]. All the above-mentioned works have common limitations, such as the lack of steady-state analysis and closed-loop stability analysis and that some works only considered SAPF without PV panels application. The main contributions of the present paper are summarized below

(i) The half-bridge SAPF-PV system is compared with the existing topologies such those studied in [3, 30, 25]. It is confirmed that the proposed structure is more robust and entails a reduced number of components hence increasing system reliability. Moreover, unlike in other works such in [25, 13, 12], the studied structure allows the integration of the PV renewable energy sources and contrubute to the decrease of the grid electricity consumption.

(ii) Unlike some previous studies [22, 14, 23] in which the controlller was designed based on a linearized model, the proposed nonlinear controller presented here is directly designed using a nonlinear model. A backstepping approach is applied in the inner loop to perform PFC. The outer-loop controller is designed using a filtered PI controller combined with a PO algorithm. The approach is demonstrated to be effective to achieve the energy exchange between the PV generator and the AC grid.

(iii) The controller performances of the SAPF-PV system are formally examined for the first time to the best knowledge of the author. Both steady-state analysis and a closed-loop stability analysis is performed on the nonlinear averaged model by using Lyapunov design approach guaranteeing the achievement of all desired objectives. Such analyses have not reported in previous works such as [10, 31, 6, 28]. The extensive simulations are performed under various operating conditions.

The remainder of the paper is structured as follows: The description and the mathematical model for SAPF-PV are presented in Section 2. The steady state analysis based on average model is developed and discussed in Section 3. The design of the nonlinear backstepping approach is provided in Section 4, while the closed-loop stability analysis is discussed in Section 5. To test the theoretical results using the proposed approach, Section 6 displays and discusses results obtained from numerical simulations performed on the detailed switched model of the system. Finally, the last section concludes the work.

2. SAPF-PV configuration and modeling

In this section, a description and mathematical modeling of the system considered in this study are presented. The system is responsible for active power filtering, maximum power extraction from the PV sources and energy injection into the grid. Its schematic diagram is shown in Fig.1. As can be seen in this figure, the system comprises three main parts detailed below

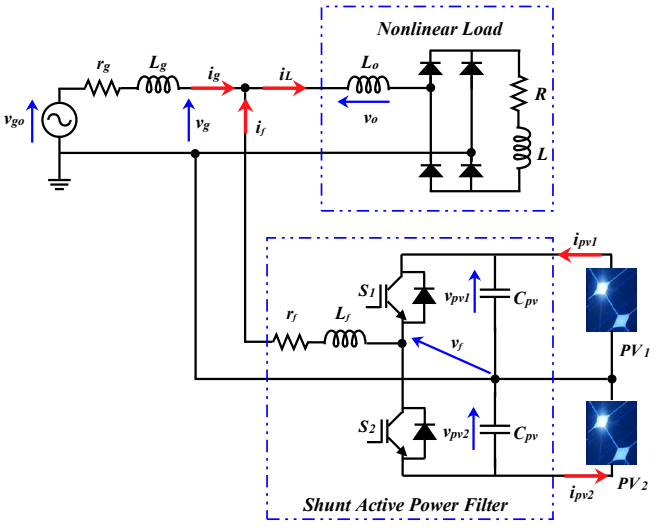

Figure 1: Schematic circuit diagram of a grid-connected single phase SAPF-PV system feeding a nonlinear load.

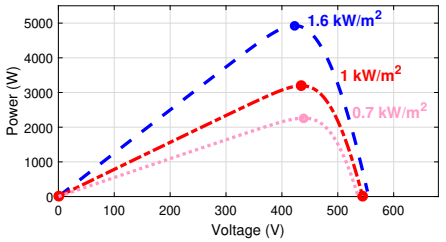

Figure 2: The P-V curves of the used PV generator at constant temperature ($T = 25°C$).

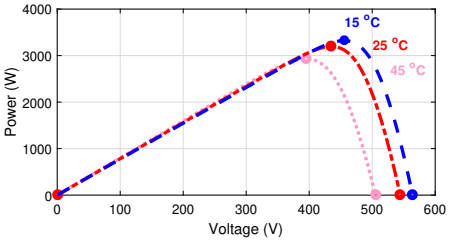

Figure 3: The P-V curves of the used PV generator at constant irradiance ($G = 1000\,\mathrm{W/m^2}$).

(i) A single-phase generator in series with an internal impedance formed by an inductor and resistor (L_g, r_g). This generator represent the power grid.

(ii) A single phase nonlinear load which is responsible for the harmonic pollution of the electrical power grid. The load consists of full bridge rectifier in parallel with an $R - L$ network.

(iii) A single phase two-stage IGBT half bridge inverter with two identical DC link capacitors C_{pv} and a filtering impedance (R_f, L_f). The inverter is fed from PV sources and is used as a SAPF.

2.1. Photovoltaic system description

In this work two similar PV panels of 1STH-215-P type are used as energy source for the SAPF. Each PV panel consists of one string of PV modules. The string is formed by $N_s = 15$ series-connected modules. The equivalent electrical parameters of the PV panel at standard functioning conditions ($G = 1000\,\mathrm{W/m^2}$, $T = 25°C$) are listed in Table I. The corresponding maximum power points (MPP) under varying environmental conditions are illustrated in Table II. The P-V curves under solar irradiance variations (1600, 1000, and $700\,\mathrm{W/m^2}$) at constant temperature ($T = 25°C$) are depicted in Fig.2. The P-V curves under temperature changes (45, 25, and $15\,°C$) at constant irradiance ($G = 1000\,\mathrm{W/m^2}$) are represented in Fig.3.

2.2. SAPF-PV system modeling

The switching decision of the inverter switches is based on pulse width modulation (PWM). Let the binary switching signals μ applied to the these swicthes of the inverter are defined as follows

$$\mu = \begin{cases} +1, \text{ if } S_1 \text{ is ON and } S_2 \text{ is OFF} \\ -1, \text{ if } S_1 \text{ is OFF and } S_2 \text{ is ON} \end{cases} \quad (1)$$

Table I
Electrical parameters of the PV panel

Parameters	Values
Maximum power voltage (V_m)	29 V
Maximum power current (I_m)	7.35 A
Maximum power (P_m)	213.15 W
Short circuit current (I_{sc})	7.84 A
Open circuit voltage (V_{oc})	36.3 V

Table II
Maximum power points (MPP)

Maximum power points	Irradiation conditions (W/m^2)	Temperature conditions ($°C$)	Maximum voltages (V)	Maximum powers (W)
$MPP1$	$G = 1000$	$T = 25$	435.01 V	3197.30 W
$MPP2$	$G = 1600$	$T = 25$	422.56 V	4930.56 W
$MPP3$	$G = 700$	$T = 25$	438.91 V	2261.70 W
$MPP4$	$G = 1000$	$T = 45$	395.04 V	2930.56 W
$MPP5$	$G = 1000$	$T = 15$	455.04 V	3321.60 W

By applying Kirchhoff's laws to the SAPF-PV system shown in Fig.1, the following differential equations describing its dynamic behavior are obtained

$$L_g \frac{di_g}{dt} = -r_g i_g + v_{go} - v_g \tag{2a}$$

$$L_f \frac{di_f}{dt} = -r_f i_f + \left(\frac{1+\mu}{2} v_{pv1} - \frac{1-\mu}{2} v_{pv2} \right) - v_g \tag{2b}$$

$$C_{pv} \frac{dv_{pv1}}{dt} = i_{pv1} - \frac{1+\mu}{2} i_f \tag{2c}$$

$$C_{pv} \frac{dv_{pv2}}{dt} = i_{pv2} + \frac{1-\mu}{2} i_f \tag{2d}$$

where i_g and v_{go} are respectively the current and the voltage of power grid, i_f stands for the filtering current injected by the SAPF and i_{pv1}, i_{pv2}, v_{pv1} and v_{pv2} are respectively the currents and the voltages produced by a PV panels.

The switched model of equations (2a)-(2d) can be used for performing accurate numerical simulation but it is not appropriate for designing the controller since its contains the binary signal μ. For designing a controller, the averaged model is conventionally used and it is obtained by averaging the state variables and the driving over each switching period [15]. In doing so, the expression of the averaged model of the SAPF-PV can be obtained by just substituting in (2a)-(2d) the electrical variables by their averages and the driving signal μ by its duty cycle u. Therefore, the averaged model of the SAPF-PV can be expressed as follows

$$L_g \frac{dx_{1,r}}{dt} = -r_g x_{1,r} + v_{go} - \overline{v}_g \tag{3a}$$

$$L_f \frac{dx_{1,f}}{dt} = -r_f x_{1,f} + \left(\frac{1+u}{2} \frac{x_{2,f} + x_{3,f}}{2} - \frac{1-u}{2} \frac{x_{2,f} - x_{3,f}}{2} \right) - \overline{v}_g \tag{3b}$$

$$C_{pv} \frac{dx_{2,f}}{dt} = i_{pv1} + i_{pv2} - u x_{1,f} \tag{3c}$$

$$C_{pv} \frac{dx_{3,f}}{dt} = i_{pv1} - i_{pv2} - x_{1,f} \tag{3d}$$

where $x_{1,r}$, $x_{1,f}$, $x_{2,f}$, $x_{3,f}$, $\bar{v}_g$ denote the average values of the variables i_g, i_f, $(v_{pv1} + v_{pv2})$, $(v_{pv1} - v_{pv2})$, v_g respectively and u stands for the duty cycle of the driving signal μ.

3. Steady state analysis

The grid voltage $v_{go}(t)$ is assumed to be sinusoidal and it can be expressed as follows

$$v_{go}(t) = E_g \sin(\omega_g t) \tag{4}$$

where E_g and ω_g stands for the magnitude and the angular frequency of grid voltage $v_{go}(t)$ respectively. In steady-state operation, the load current $i_L(t)$ can be expanded as a Fourier series as follows

$$i_L(t) = \sum_{h=1}^{\infty} I_{Lh} \sin(h\omega_g t + \varphi_h) \tag{5}$$

where φ_h and I_{Lh} are the phase and the magnitude of the h-th harmonic component, respectively, of the current $i_L(t)$.

It is aimed that, in steady state, the grid current have a pure sinusoidal waveform in phase with the grid voltage, i.e, it is desired that

$$x_{1,r}(t) = \beta E_g \sin(\omega_g t) \tag{6}$$

where β is a dynamic conductance setting the amplitude of the grid current. The SAPF-PV system provides the total harmonic and reactive currents according to the following equation

$$x_{1,f}(t) = i_L(t) - x_{1,r}(t) \tag{7}$$

Substituting (4) and (6) in (3a), one can easily obtain that the voltage $\overline{v}_g(t)$ can be expressed as follows

$$\overline{v}_g(t) = V_g \sin(\omega_g t - \theta_1) \tag{8}$$

where the amplitude V_g and the phase θ_1 of $\overline{v}_g(t)$ are given by

$$V_g = E_g \sqrt{(1 - r_g\beta)^2 + (\beta L_g \omega_g)^2}, \quad \theta_1 = \arctan\left(\frac{\beta L_g \omega_g}{1 - r_g\beta}\right)$$

Based on (7) and using (5), the following expression of $x_{1,f}(t)$, in steady-state regime, is obtained

$$x_{1,f}(t) = I_f \sin(\omega_g t + \theta_2) + \sum_{h=2}^{\infty} I_{Lh} \sin(h\omega_g t + \varphi_h) \tag{9}$$

where the amplitude I_f and the phase θ_2 of $x_{1,f}(t)$ are given by

$$I_f = \sqrt{(I_{L1}\cos(\varphi_1) - \beta E_g)^2 + (I_{L1}\sin(\varphi_1))^2}$$
$$\theta_2 = \arctan\left(\frac{I_{L1}\sin(\varphi_1)}{I_{L1}\cos(\varphi_1) - \beta E_g}\right)$$

Using (3b) and (8)-(9) one has

$$\bar{v}_f(t) = V_f \sin(\omega_g t + \theta_3) + \sum_{h=2}^{\infty} I_{Lh} \sin(h\omega_g t + \theta_4) \tag{10}$$

where V_f, θ_3 and θ_4 are given by

$$V_f = \sqrt{(\psi_1)^2 + (\psi_2)^2}, \theta_3 = \arctan\left(\frac{\psi_2}{\psi_1}\right), \theta_4 = \arctan\left(\frac{\psi_4}{\psi_3}\right)$$

In turn, the parameters ψ_1, ψ_2, ψ_3 and ψ_4 are as follows

$$\psi_1 = \cos(\theta_2) r_f I_f + \cos(\theta_1) V_g + L_f I_f \omega_g \sin(\theta_2)$$
$$\psi_2 = L_f I_f \omega_g \cos(\theta_2) - \sin(\theta_2) r_f I_f - V_g \sin(\theta_1)$$
$$\psi_3 = r_f \cos(\varphi_h) - L_f \omega_g h \sin(\varphi_h)$$
$$\psi_4 = r_f \sin(\varphi_h) + L_f \omega_g h \cos(\varphi_h)$$

Using (3c)-(3d), the following equation is obtained

$$C_{pv} \frac{d x_{2,f}^2}{dt} = 4 P_{pv} + 2 x_{1,f} \bar{v}_f \tag{11}$$

Let $\chi = x_{2,f}^2$. Substituting (9)-(10) in the previous equation, one obtains

$$C_{pv} \frac{d\chi}{dt} = 4 P_{pv} - f_1(\beta) + f_2(\beta) \tag{12}$$

where $f_1(\beta)$ is time-independent function and $f_2(\beta)$ is a time varying function that can be expressed as follows

$$f_1(\beta) = 2 I_f V_f \cos(\theta_2 - \theta_3)$$
$$f_2(\beta) = 2 I_f V_f \cos(2\omega_g t + \theta_2 + \theta_3)$$

It is worth to notice that the DC component of the time varying function $f_2(\beta)$ is zero.

Remark 1. *It can be demonstrated that in steady state the DC bus voltage contains a DC component and AC term oscillating at the double of the grid frequency. In practice, due to the low pass filtering characteristics, high order harmonic components larger than 2 can be neglected.*

By averaging (12) over one grid cycle, one obtains the following averaged state equation describing the dynamics of χ

$$C_{pv} \frac{d\bar{\chi}}{dt} = 4 P_{pv} - f_1(\beta) \tag{13}$$

Remark 2. *In steady-state one has $\frac{d\bar{\chi}}{dt} = 0$ and therefore $P_{pv} = f_1(\beta)/4$. This condition reflects the ideal power balance between the solar PV panels and the grid.*

Solving (13) for $\bar{\chi}$, one gets

$$\bar{\chi}(t) = \frac{1}{C_{pv}} (4 P_{pv} - f_1(\beta)) t + \chi_{pv} \tag{14}$$

where χ_{pv} indicates the square of the PV voltage.

Remark 3. *As a consequence, the evolution of the DC bus voltage is completely guaranteed by the additional signal β. Indeed, the signal β can increase or decrease the DC bus voltage and consequently destabilizing the whole system. For this reason, the signal β will be generated by the outer loop which must permanently guaranty the equality $4 P_{pv} = f_1(\beta)$ and therefore maintaining the power balance between the solar PV panels and the grid in a addition to the load.*

Based on $\bar{v}_f = [(1+u)(x_{2,f} + x_{3,f}) - (1-u)(x_{2,f} - x_{3,f})]/2$ and using (10), the equation of the control law u^* enabling the power factor requirement is given by:

$$u^* = \frac{2 V_f}{x_{2,f}} \sin(\omega_g t + \theta_3) \tag{15}$$

where V_f is very close to E_g (r_g, L_g, r_f and L_f are negligible) in practice. Since the control variable $u^* \in (-1, 1)$, by considering only the DC term of $x_{2,f}$ and neglecting its high order harmonics, it can be concluded that the DC bus voltage should be higher than twice the amplitude of the grid voltage, i.e, the following inequality must hold:

$$x_{2,f} > 2 E_g \tag{16}$$

4. Controller design

In this paper, we seek for a control strategy that simultaneously addresses the three control objectives: (i) forcing the grid current to be sinusoidal waveform and in phase with the grid voltage by compensating for reactive power and undesired harmonic contents; (ii) extracting the maximum PV power by applying an MPPT algorithm and (iii) achieving the maximum energy exchange from the solar PV generator to the AC grid source by regulating the voltage of the DC link capacitors. The proposed controller design for the SAPF-PV system comprises two cascaded loops (inner loop and outer loop) as illustrated in Fig.4.

4.1. Inner loop design

To perform PFC, the input current $x_{1,r}$ supplied by the electrical power grid should follow a reference signal which is proportional to grid voltage, i.e, $x^*_{1,r} = \beta v_{go}$. Indeed, it can be observed that this can be achieved if the filter current $x_{1,f}$ injected by SAPF-PV system match, as neatly as possible, the reference signal $x^*_{1,f}$ defined by

$$x^*_{1,f} = i_L - \beta v_{go} \tag{17}$$

The inner controller will be designed using Backstepping approach to achieve PFC asymptotically. Now, let us introduce the following tracking error associated to the filter current $x_{1,f}$:

$$z_1 = x_{1,f} - x^*_{1,f} \tag{18}$$

Based on (18) and using (3b), one gets the following equation

$$\dot{z}_1 = -r_f x_{1,f} + \frac{1}{2} x_{3,f} + \frac{1}{2} u x_{2,f} - \bar{v}_g - L_f \dot{x}^*_{1,f} \tag{19}$$

The control variable u has emerged in (19) after differentiating the tracking error, then the control law of the current controller will be determined in a single step. To this regard, a simple Lyapunov function candidate is

$$V = \frac{1}{2} z_1^2 \tag{20}$$

Its time derivative is given by:

$$\dot{V} = \dot{z}_1 z_1 \tag{21}$$

For the z-system described by (19) to be globally asymptotically stable, it is enough to select the control variable u so that $\dot{V} = z_1^2 c_1$ which, due to (21), ensures the following equality

$$\dot{z}_1 = -c_1 z_1 \tag{22}$$

where $c_1 > 0$ is a design parameter. Combining (19) and (22) gives the following Backstepping control law

$$u = \frac{2}{x_{2,f}} \left[r_f x_{1,f} - \frac{1}{2} x_{3,f} + \bar{v}_g + L_f \dot{x}^*_{1,f} - c_1 z_1 \right] \tag{23}$$

Proposition 1: *Consider the SAPF-PV system represented by Fig.1, consisting of the subsystem (3a)-(3d) and the inner control law (23). If β and its first derivative $\dot{\beta}$ are obtainable, the inner loop undergoes, in z_1-coordinate the following equation:*

$$\dot{z}_1 = -c_1 z_1 \tag{24}$$

Remark 4.

1) *As mentioned previously, it shown from inner control law (23) that β and its first derivative $\dot{\beta}$ must be obtainable to conclude that the PFC purpose is realized. In fact, the signal β is not known a priori but it will be produced by the outer loop to achieve voltage controller at the terminals of the solar PV panels (subsection 4.2). Then, it will be scheduled later (see Theorem) that the signal β converges to a steady-state value ensuring the PFC requirement.*
2) *Although the load current derivative di_L/dt must be measurable for the inner control law in order to be implemented, in practice, this can be determined from the inductor voltage v_o.*

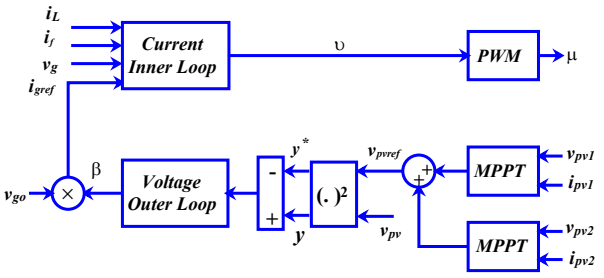

Figure 4: Block diagram of the designed controller.

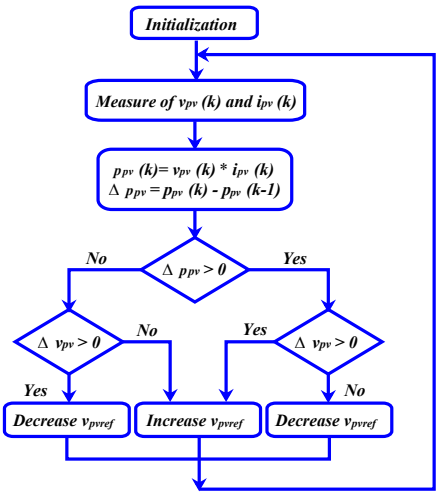

Figure 5: Flowchart of the perturb-and-observe algorithm MPPT.

4.2. Outer loop design

4.2.1. PV generator reference voltage

The DC link voltage is regulated to a desired value using an outer voltage loop. Particularly, the solar PV voltage $x_{2,f}$ will be controlled to its maximum tracking signal $x^*_{2,f}$ delivered by an MPPT algorithm. For this, the PO algorithm is chosen due to its simplicity of implementation. This algorithm uses a periodic perturbation of the PV operating voltage hence imposing the system to oscillate in the close vicinity of the MPP. The amplitude of this oscillation can be controlled by the value of the perturbation amplitude of the perturbed variable. The flowchart of the MPPT algorithm are illustrated in Fig.5.

4.2.2. DC bus voltage regulation

As stated before, without PV voltage regulation, this voltage does not converge to a constant value unless the value of β is selected such that $4P_{pv} = f_1(\beta)$. Otherwise, the transfer of energy from the PV panels to the electrical grid cannot be achieved. For this purpose, a control law for the variable β will be created so that the solar PV voltage $x_{2,f}$ is controlled to its reference $x^*_{2,f}$ given by the MPPT algorithm.

a) *Relation between β and $x_{2,f}$:*
First, we need to establish a dynamic relationship between the variable β and the PV voltage $x_{2,f}$ in the following proposition.
Proposition 2: *Consider the SAPF-PV system represented by Fig.1, consisting of the subsystem (3a)-(3d) with the inner control law given by (23). For simplicity, it is assumed that the two PV panels have the same characteristics ($p_{pv1} = p_{pv2} = p_{pv}$) and the inner loop controller is much faster than the outer loop controller such that for designing the outer loop it is assumed that ($x^*_{1,r} = \beta v_{go}$). Then, the following statements hold*
1) *The PV voltage $x_{2,f}$ is related to the variable β by the following equation*

$$\frac{dx_{2,f}}{dt} = \frac{2i_{pv}}{C_{pv}} - \frac{1}{x_{2,f}}[f_1(\beta,\dot{\beta},z_1) + f_2(\beta,\dot{\beta},z_1,t)] \tag{25}$$

2) *Then, the variable $y = x^2_{2,f}$ is described by the following first order time-varying linear equation*

$$\frac{dy}{dt} = \frac{4p_{pv}}{C_{pv}} - [f_1(\beta,\dot{\beta},z_1) + f_2(\beta,\dot{\beta},z_1,t)] \tag{26}$$

where the function $f_1(\beta,\dot{\beta},z_1)$ and $f_2(\beta,\dot{\beta},z_1,t)$ are indicated in the Section 8 (Appendix A).
Proof. The expression (25) can be obtained by replacing in (3c) u by its expression given by (23). Then the expression (26) is derived by differentiating the squared voltage y expression and using (24).

b) *Squared voltage controller*

We aim to design an appropriate outer control law so that the squared voltage $y = x_{2,f}^2$ tracks precisely a desired reference $y^* = x_{2,f}^{*2}$. Considering that the control signal β and its derivative are obtainable (see Remark 4), we use the following filtered PI controller:

$$\beta = \frac{c_4}{c_4 + s}(c_2 Z_2(s) + c_3 Z_3(s)) \tag{27}$$

with

$$z_2(t) = y^*(t) - y(t),\ z_3(t) = \int_0^t z_2(\tau) d\tau$$

where $Z_2(s)$ and $Z_3(s)$ stand for the Laplace transforms of the variables $z_2(t)$ and $z_3(t)$ respectively. At this stage, the controller parameters (c_2, c_3, c_4) are any positive real constants. In the next section these parameters will be determined so that the control objectives can be attained. From (27) the differential equation relating the variable β to other state variables of the system is

$$\dot{\beta} = c_4(c_2 z_2 + c_3 z_3 - \beta) \tag{28}$$

5. Control system analysis

Now, the control system analysis will be developed using the averaging theory, and Routh-Hurwitz stability criterion [20]. The next theorem demonstrates that the control objectives are attainable on average with a high accuracy degree which relies significantly on the grid frequency ω_g. The following notations are needed for formulating the results

$$\begin{aligned}
&z_4 = \beta,\ \varepsilon = 1/\omega_g \\
&k_1 = E_g^2(r_f + r_g) \\
&k_2 = E_g^2 - E_g I_{L1}(\cos(\varphi_1)(r_g - 2r_f) - L_g \omega_g \sin(\varphi_1)) \\
&k_3 = E_g I_{L1}(\cos(\varphi_1) + \sin(\varphi_1)) - 4p_{pv} \\
&k_4 = \frac{E_g L_f}{C_{pv}}(\beta_0 E_g - I_{L1}\cos(\varphi_1)) \\
&k_5 = \frac{E_g}{C_{pv}}[E_g(2\beta_0(1 + r_g) - 1 - L_f \beta_0 c_4) + I_{L1}(r_g \\
&- 2r_f + L_f \cos(\varphi_1)] \\
&a_0 = c_1 c_3 c_4(k_5 - c_4 k_4) \\
&a_1 = c_4[c_3(k_5 - k_4) + c_1(c_2 k_5 - (c_2 c_4 + c_3)k_4] \\
&a_2 = c_4[c_2(k_5 - c_4 k_4) - c_3 k_4 + c_1(1 - c_2 k_4)] \\
&a_3 = c_1 + c_4(1 - c_2 k_4)
\end{aligned}$$

Theorem (main result): *Consider the SAPF-PV system as illustrated in Fig.1, consisting of the subsystem (3a)-(3d) with nonlinear controller, including the following components:*

- *The current control law (23), with positive parameter* c_1.
- *The voltage control law (27) with positive constants* (c_2, c_3, c_4).

After that, the control system analysis has the following features:

1. The following error $z_1 = x_{1,f} - x_{1,f}^*$ disappears exponentially rapid, with $x_{1,f}^* = \beta v_{go}$.

2. Introduce the enhanced state vector Z as follows:

$$Z = \begin{pmatrix} z_1 & z_2 & z_3 & z_4 \end{pmatrix}^T$$

The state vector Z then undergoes the state equation as follows:

$$\dot{Z}(t) = f(t, Z) \tag{29}$$

where

$$f(t, Z) = \begin{pmatrix} -c_1 z_1 \\ -\frac{4p_{pv}}{C_{pv}} + f_1(Z) + f_2(Z, t) \\ z_2 \\ c_4(c_2 z_2 + c_3 z_3 - z_4) \end{pmatrix}$$

3. Let prove the following inequalities by selecting the appropriate controller design parameters (c_1, c_2, c_3, c_4):

$$a_0 > 0,\ a_3 > 0,\ a_3 a_2 - a_1 > 0,\ a_1 a_2 a_3 - a_1^2 - a_0 a_3^2 > 0 \tag{30}$$

For all $0 < \varepsilon < \varepsilon^*$, the state equation (29) has a unique exponentially stable π/ω_g-periodic solution $\bar{Z}(t, \varepsilon)$ with the condition $\| \bar{Z}(t, \varepsilon) - W_0^* \leqslant \delta^* \varepsilon \|$, where ε^* and δ^* are positive constants.

with $Z = \begin{pmatrix} 0 & 0 & \frac{\beta_0}{c_3} & \beta_0 \end{pmatrix}^T$

See Section 8 (Part B) for the Proof of previous theorem.

Remark 5.

1) *Equations (27) and (28) indicate that β and its first derivative may be computed utilizing the obtainable signals, which ensures that the errors z_3 and z_4 are clearly time-differentiable. Moreover, the results of Proposition 1 prove that the error z_1 yields the Eq.(24), which is globally asymptotically stable.*
2) *The enhanced state vector equation (29) is immediately got by (26)-(28).*
3) *The previous theorem demonstrates that, under condition (30), the undesired harmonic mitigation is effectively reached in the mean value with a precision degree according to the value of $\varepsilon = 1/\omega_g$. It also proves that β meets (up to small ripple) to a constant value, then assuring the PFC fulfillment. the output voltage regulation goal is reached in the mean value with a high precision, which is based on the grid voltage frequency ω_g. The used frequency $\omega_g = 50Hz$ allows for tight voltage regulation and excellent PFC performance.*

6. Numerical simulation

The complete plant system and the controller are described in Fig. 6 and simulated in Matlab/Simulink environment, using the fixed-step solver ODE14x (Extrapolation). For simulation process, the used nonlinear load is highly inductive. The parameter values of the power system and the controller design are summarized in Tables III and IV. To test the robustness of the closed-loop control system performance, some of the important features are considered:

- Performance evaluation with standard climatic conditions.
- Performance evaluation with solar irradiation conditions.
- Performance evaluation with temperature conditions.

6.1. Performance evaluation with standard climatic conditions

In this case, the performance evaluation is conducted under standard climatic conditions ($G = 1000\,\mathrm{W/m^2}, T = 25°C$) as illustrated in Figs.7-15. Fig.7 illustrates the waveform of the load current, which shows obviously a harmonic distortion caused by a nonlinear load with a THD value of 39.73% as illustrated by Fig.8. The resulting controller performances are illustrated by Fig.9-15. The PV voltage tracks well its maximum reference after a brief transition period as indicated in Fig.9, which confirming the results of the previous Theorem. The produced PV power is completely distributed into the electrical source as illustrated in Fig.10. The filter current injected from SAPF into the electrical

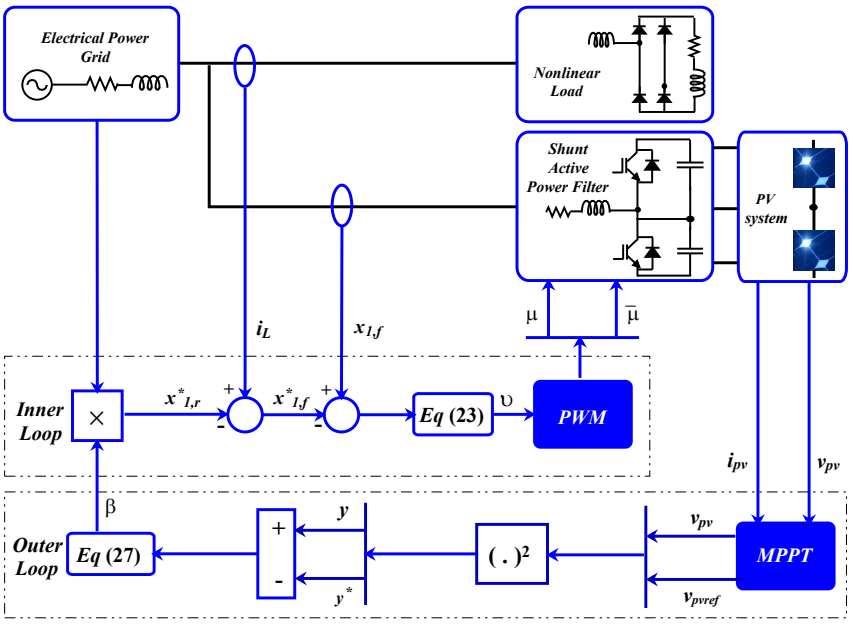

Figure 6: Block diagram of the complete simulated control system

Table III
SAPF-PV system characteristics.

Parameter	Symbol	Value
Power grid	v_{go}	$230\sqrt{2}$ V / 50 Hz
	r_g	2 mΩ
	L_g	0.2 mH
Nonlinear load	L_0	500 mH
	R/L	5 Ω / 1 mH
PV system	N_p	1
	N_s	15
Shunt active power filter	C_{pv}	10 μF
	L_f	3 mH
	R_f	8 mΩ
PWM switching frequency	f_{PWM}	10 kHz

Table IV
Controller design coefficients.

Parameter	Symbol	Value
Current regulator (PFC)	c_1	7×10^4
DC link voltage regulator	c_2	$1 \times 10^{-2} V^{-2} \Omega^{-1}$
	c_3	$2 \times 10^{-3} V^{-2} \Omega^{-1} s^{-1}$
	c_4	$5000 \times s^{-1}$

source tracks its reference with high accuracy, providing quick dynamic response and very good steady-state behavior of nonlinear backstepping controller as shown in Fig.11. Indeed, it is observed in Fig.12 that, the grid current is perfectly sinusoidal, which the undesired harmonic contents are well mitigated as shown in Fig.13 and the source voltage remains in phase with the grid current as illustrated in Fig.14. Finally, Fig.15 indicates that the average of signal β becomes rapidly constant. as result, a unity PFC is attained.

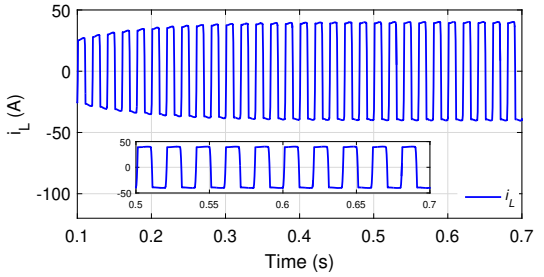

Figure 7: The load current i_L waveform.

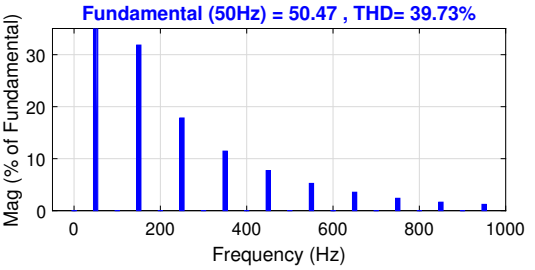

Figure 8: The harmonic content of the load current.

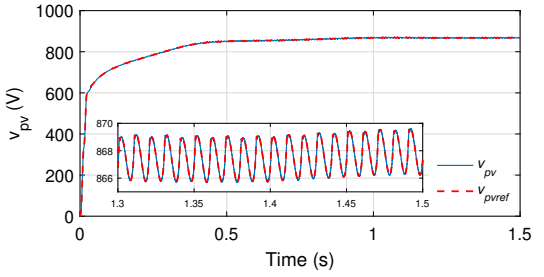

Figure 9: The PV voltage v_{pv} and its reference v_{pvref}.

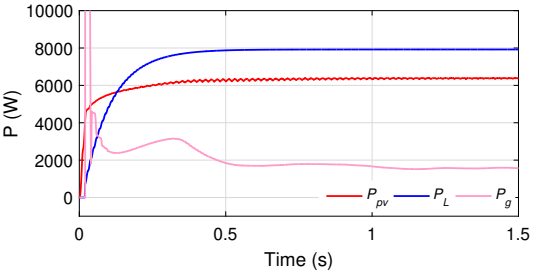

Figure 10: The generated PV panels power p_{pv}.

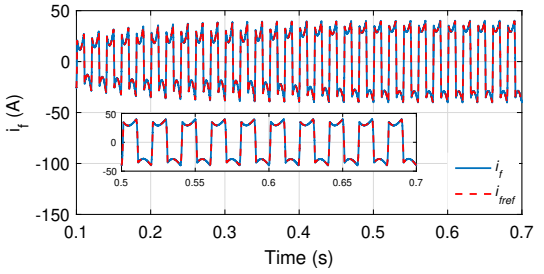

Figure 11: Filter current i_f and its reference i_{fref}.

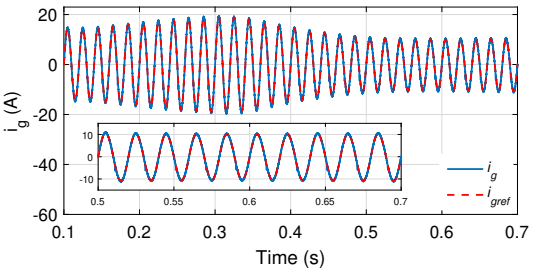

Figure 12: The grid current i_g and its reference i_{gref}.

6.2. Performance evaluation with solar irradiation conditions

The behavior of PV solar panels can be influenced by varying atmospheric conditions at daytime. The above control system performances is tested considering the varying conditions of solar irradiance with a particular irradiance pattern as illustrated in Fig.16. More precisely, the irradiance G reduced quickly from 1000 $\mathrm{W/m^2}$ to 700 $\mathrm{W/m^2}$ at time 0.5s and goes slowly from 700 $\mathrm{W/m^2}$ to 1600 $\mathrm{W/m^2}$ at time 0.8 s whereas the temperature is remained constant $T = 25°C$. It is observed from Figs.17-24 that, the nonlinear designed controller maintains the overall system in the optimal operating conditions with regard to irradiance variations. Indeed, the PV voltage follows well its maximum voltage after a brief transition periods as indicated in Fig.17. It can be seen from Fig.18 that the injected filter current converges in the mean to its reference current with a high precision. Furthermore, Fig.19 shows that the grid current keeps its sinusoidal waveform at all instants and THD value is measured as 2.60% as presented in Fig.20. The grid current and the grid voltage are actually in phase despite the solar irradiance variation as shown in Fig.21, confirming thus the PFC fulfillment. Hence, the average of signal β becomes constant each time the PFC is warranted as shown in Fig.22. Finally, Fig.23 shows the good MPPT tracking in spite of solar irradiance variation. Indeed, It is shown that the quantity of PV power is varied (see Table II), depending on the solar irradiation changing.

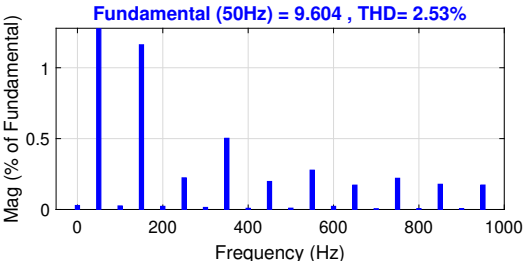

Figure 13: The harmonic content of the grid current.

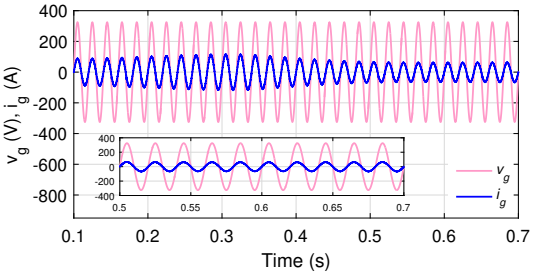

Figure 14: The rid voltage and current showing the near unity power factor.

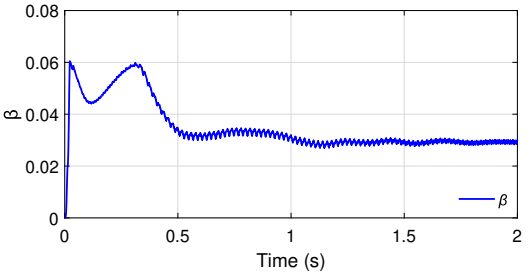

Figure 15: The external control signal β.

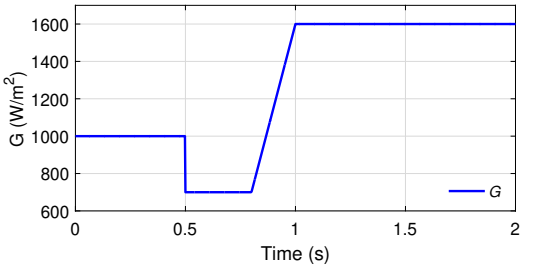

Figure 16: The used irradiation variation profile.

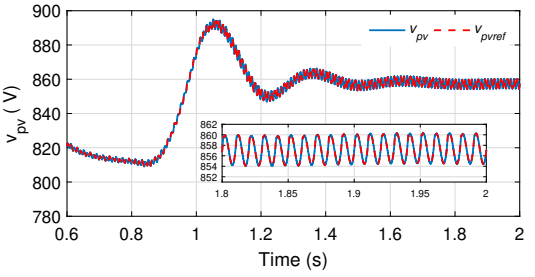

Figure 17: PV voltage v_{pv} under irradiation change.

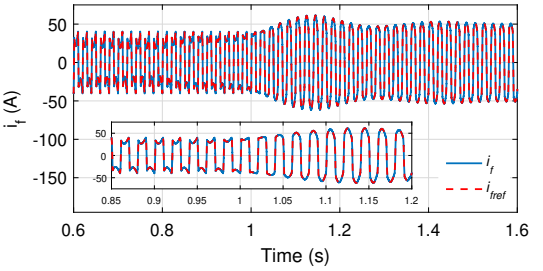

Figure 18: Filter current i_f under irradiation change.

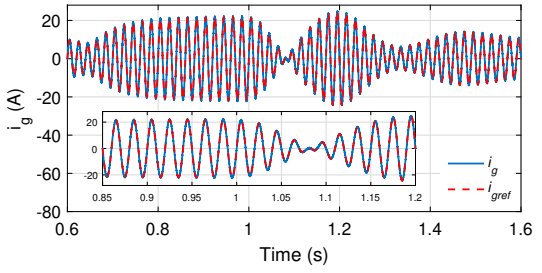

Figure 19: The grid current i_g under irradiation change

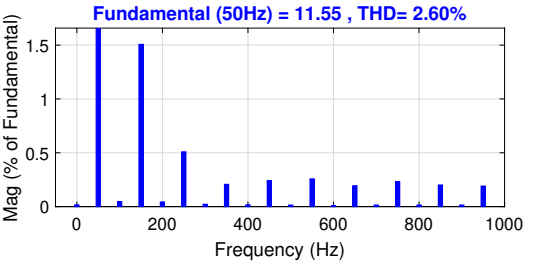

Figure 20: THD of the grid current under irradiation change

6.3. Performance evaluation with temperature conditions

Figs.24-31 illustrate the behavior of the closed-loop controller in the presence of temperature variations with a particular temperature pattern as shown in Fig.24. More precisely, the temperature T has augmented rapidly from $25°C$ to $45°C$ at time $0.5s$ and reduced slowly from $45°C$ to $15°C$ at time $0.8s$, whereas the irradiance G is remained constant and equal to $1000\mathrm{W/m^2}$. Fig.25 shows the good MPPT tracking of maximum voltage according to the

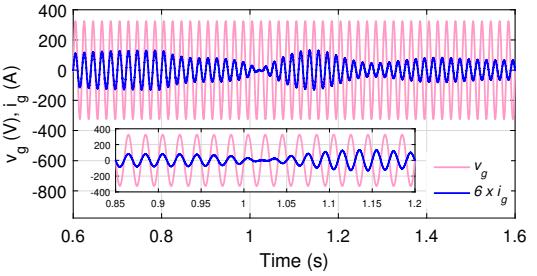

Figure 21: The grid voltage and current showing near unity power factor under irradiation change.

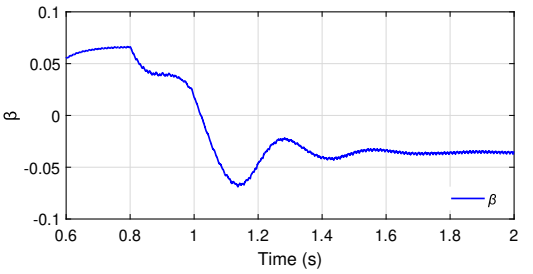

Figure 22: External control signal β under irradiation change.

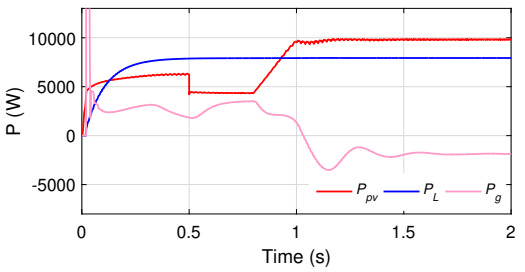

Figure 23: The PV power production under irradiation change.

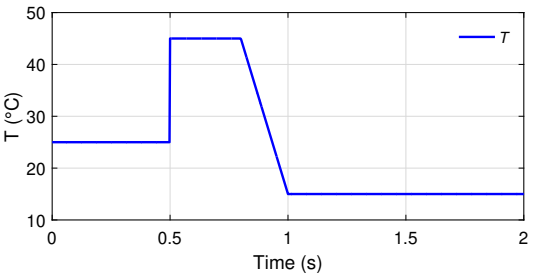

Figure 24: The used temperature variation profile.

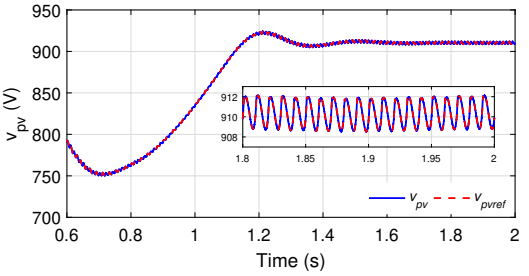

Figure 25: The PV voltage v_{pv} under temperature change.

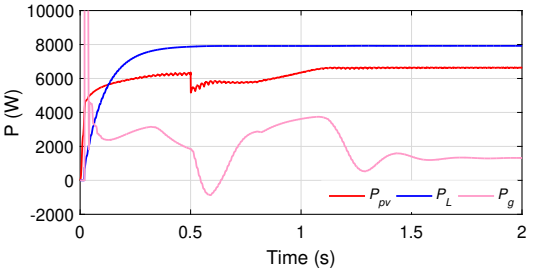

Figure 26: The PV power p_{pv} under temperature change.

temperature variations. Indeed, the extracted solar PV power curve changes (see Table II) as illustrated in Fig.26. The injected filter current converges each instants to its reference current with a high precision under temperature variation as illustrated in Fig.27. It can be seen in Fig.28 that the grid current remains a sinusoidal waveform and the THD value is equal to $2,87\%$ as presented in Fig.29. The source voltage kept in phase with grid current, proving the PFC achievement as shown in Fig.30. This is also proved by Fig.31, which indicates that the average of signal β becomes constant according to the temperature variations, and verifying the fulfillment of unitary power factor.

7. Conclusion

In this work, we have studied the problem of controlling a single-phase shunt active power filter interfacing renewable energy source and the electrical power grid. A nonlinear control strategy based on the Backstepping approach was developed for the SAPF-PV system. According to the theoretical analysis and the obtained numerical results, it has been formally proved that the controller objectives are actually achieved in the mean including extraction of maximum active power from the PV panels, regulation of DC-link voltage, and PFC achievement. The designed inner loop controller has been successfully controlling the SAPF-PV system to ensure a better PFC realization under tolerable THD coefficient, and limited to within IEEE standard 519. The designed outer loop controller provides perfect PI controller of the PV voltage to a given maximum voltage created by the MPPT skills, which warranty the power

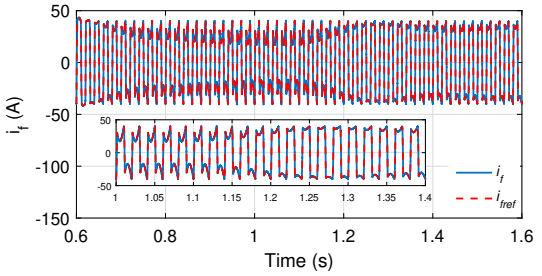

Figure 27: The Filter current i_f under temperature change.

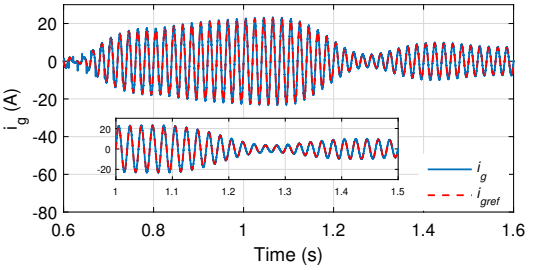

Figure 28: The grid current i_g under temperature change.

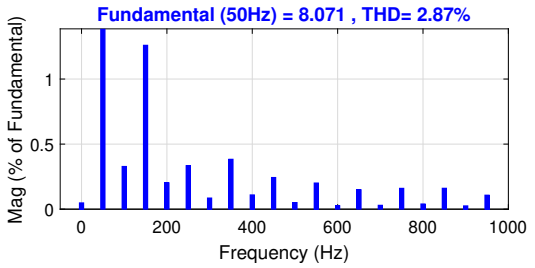

Figure 29: The THD of the grid current under temperature change.

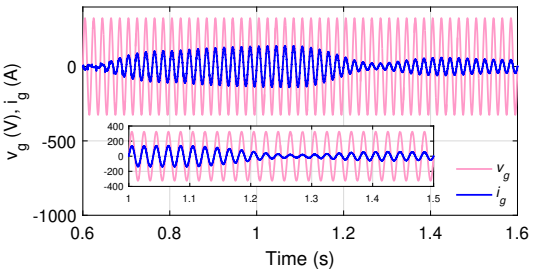

Figure 30: The grid voltage and current showing near unity power factor under temperature change.

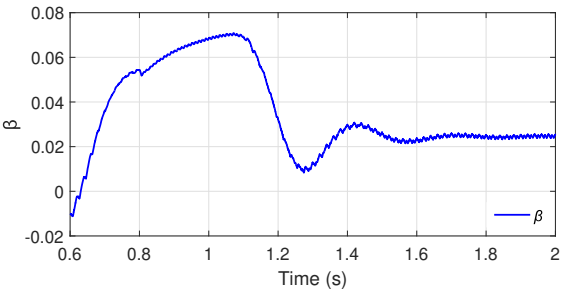

Figure 31: The external control signal β under temperature change.

exchange between the PV panels and the electrical power grid. Finally, the overall control system performances is achieved according to the stability analysis and averaging theory.

8. Appendix

A. **Proof of Relation between β and $x_{2,f}$**

$$f_1(\beta,\dot{\beta},z_1)=\frac{E_g I_{L1}}{C_{pv}}[(1-2r_f\beta+r_g\beta-L_f\dot{\beta})\cos(\varphi_1)+(1-\beta L_g\omega_g)\sin(\varphi_1)]+\frac{\beta E_g^2}{C_{pv}}[r_f\beta-1+r_g\beta+L_f\dot{\beta}]+$$

$$\frac{2z_1}{C_{pv}}(r_f z_1+r_g z_1-c_1 z_1)$$

$$f_2(\beta,\dot{\beta},z_1,t)=\frac{2E_g}{C_{pv}}(1-2r_f\beta-r_g\beta-\beta L_g\omega_g-L_f\dot{\beta}-L_f\beta\omega_g)\sum_{h=1}^{\infty}I_{Lh}\sin(h\omega_g t+\varphi_h)\sin(\omega_g t)+\frac{2E_g}{C_{pv}}[(-2r_f z_1\beta$$

$$-\beta r_g z_1+z_1 r_g\beta-L_f\beta\frac{di_L}{dt}-L_f z_1\dot{\beta}+c_1 z_1\beta)\sin(\omega_g t)+(-z_1\beta L_g\omega_g-L_f\beta\omega_g z_1)+\frac{2E_g}{C_{pv}}[(-2r_f z_1\beta-\beta r_g z_1+z_1 r_g\beta-$$

$$L_f\beta\frac{di_L}{dt}-L_f z_1\dot{\beta}+c_1 z_1\beta)\sin(\omega_g t)+(-z_1\beta L_g\omega_g-L_f\beta\omega_g z_1)\cos(\omega_g t)]+\frac{\beta E_g^2}{C_{pv}}[(\beta L_g\omega_g+L_f\beta\omega_g)\sin(2\omega_g t)+(1-r_f\beta-$$

$$r_g\beta-L_f\dot{\beta})\cos(2\omega_g t)]+\frac{E_g I_{L1}}{Cpv}[(-\beta L_g\omega_g+1)\sin(2\omega_g t+\varphi_1)-(2r_f\beta+1)\cos(2\omega_g t+\varphi_1)]$$

B. **Proof of Theorem**

Stability analysis of the above system (29) is dealt with using averaging theory [15]. For this purpose, we insert the time-scale change $\tau=\omega_g t$. It results from (30) that $W(\tau)\overset{def}{=}W(t)=W(\tau/\omega_g)$ follows the differential equation:

$$\dot{W}(\tau)=\varepsilon\, g(\tau,\, W,\, \varepsilon) \tag{31}$$

where $\dot{W}$ indicates the derivative with respect to τ, and

$$g(\tau,\, W,\, \varepsilon)=\begin{pmatrix} -c_1 w_1 \\ -\frac{4p_{pv}}{C_{pv}}+g_1(W)+g_2(W,\,\tau,\,\varepsilon) \\ w_2 \\ c_4(c_2 w_2+c_3 w_3-w_4)\end{pmatrix} \tag{32}$$

with

$$g_1(W(\tau))\overset{def}{=}f_1(Z(t))=f_1(W(\tau))$$

$$g_2(W(\tau),\,\tau,\,\varepsilon))\overset{def}{=}f_2(Z(t),,t)=f_2(W(\tau),\,\tau,\,\varepsilon)$$

It also appears from (26) and (32) that $g(\tau,\, W_0,\, \varepsilon)$ as a function of τ is periodic with period 2π. Now, let us introduce the average function $g_0(W_0)$:

$$g_0(W_0)\overset{def}{=}\lim_{\varepsilon\to 0}\frac{1}{2\pi}\int_0^{2\pi}g(\tau,\, W_0,\, \varepsilon)d\tau,\; W_0\epsilon\Re^4 \tag{33}$$

It is easily seen from (26) and (32) that:

$$g_0(W_0)=\begin{pmatrix} -c_1 w_{1,0} \\ -\frac{4p_{pv}}{C_{pv}}+g_{1,0}(W) \\ w_{2,0} \\ c_4(c_2 w_{2,0}+c_3 w_{3,0}-w_{4,0})\end{pmatrix} \tag{34}$$

where

$$g_{1,0}(W_0) \overset{def}{=} \lim_{\varepsilon \to 0} \frac{1}{2\pi} \int_0^{2\pi} g_1(W(\tau))d\tau = \frac{w_{4,0}E_g^2}{C_{pv}}[r_f w_{4,0} -$$
$$1 + r_g w_{4,0} + L_f(c_4(c_2 w_{2,0} + c_3 w_{3,0} - w_{4,0}))] + \frac{E_g I_{L1}}{C_{pv}}[(1 -$$
$$2r_f w_{4,0} + r_g w_{4,0} - L_f(c_4(c_2 w_{2,0} + c_3 w_{3,0} - w_{4,0}))\cos(\varphi_1) +$$
$$(1 - w_{4,0}L_g\omega_g)\sin(\varphi_1)] + \frac{2w_{1,0}}{C_{pv}}(r_f w_{1,0} + r_g w_{1,0} - c_1 w_{1,0})$$
$$g_{2,0}(W_0, \tau) \overset{def}{=} \lim_{\varepsilon \to 0} \frac{1}{2\pi} \int_0^{2\pi} g_2(\tau, W, \varepsilon))d\tau = 0$$

Regarding the system (31) and according to the averaging theory [20], it is suitable to analyze the following averaged system:

$$\dot{W}_0 = \varepsilon g_0(W_0) \tag{35}$$

To this end, let us note that, for a given (34), the time-invariant system (35) has a unique equilibrium at:

$$W_0^* = \begin{pmatrix} 0 & 0 & \frac{\beta_0}{c_3} & \beta_0 \end{pmatrix}^T \tag{36}$$

with

$$\beta_0 = \frac{k_2 - \sqrt{k_2^2 - 4k_1k_3}}{2k_1} \tag{37}$$

Now, the stability of the equilibrium $W_0^* = W_0$ will be analyzed through indirect Lyapunov method [20]. Therefore, one investigates if the Jacobian of the function $g_0(.)$, at $W_0^* = W_0$ is Hurwitz. According to (34) and (35), it is easily verified that the Jacobian is defined by:

$$A = \begin{pmatrix} -c_1 & 0 & 0 & 0 \\ 0 & c_2c_4k_4 & c_3c_4k_4 & k_5 \\ 0 & 1 & 0 & 0 \\ 0 & c_2c_4 & c_3c_4 & -c_4 \end{pmatrix} \tag{38}$$

The equilibrium W_0^* will be globally exponentially stable if the matrix A is Hurwitz. To this end, the characteristic polynomial equation is given as follows:

$$\pi(\lambda) = \lambda^4 + a_3\lambda^3 + a_2\lambda^2 + a_1\lambda + a_0 \tag{39}$$

By using Routh's algebraic criteria, it implies that all the zeros of the polynomial (39) have negative real parts whether the conditions (30) are met. In other words, under these conditions, it proves that the matrix A is actually Hurwitz. Furthermore, by Lyapunov's indirect method, the equilibrium $W_0^* = W_0$ of (35) is exponentially stable.

References

[1] Abouelmahjoub, Y., Giri, F., Abouloifa, A., Chaoui, F.Z., Kissaoui, M., 2018. Adaptive Nonlinear Control of Reduced-Part three-Phase Shunt Active Power Filters: Adaptive Nonlinear Control of Reduced-Part Three-Phase Shunt Active Power Filters. Asian Journal of Control 20, 1720–1733. doi:10.1002/asjc.1681.

[2] Abouloifa, A., Aouadi, C., Lachkar, I., Boussairi, Y., Aourir, M., Hamdoun, A., 2018. Output-Feedback Nonlinear Adaptive Control Strategy of the Single-Phase Grid-Connected Photovoltaic System. Journal of Solar Energy 2018, 1–14. doi:10.1155/2018/6791056.

[3] Abouloifa, A., Giri, F., Lachkar, I., Chaoui, F.Z., Kissaoui, M., Abouelmahjoub, Y., 2014. Cascade nonlinear control of shunt active power filters with average performance analysis. Control Engineering Practice 26, 211–221. doi:10.1016/j.conengprac.2014.01.017.

[4] Ahmed, J., Salam, Z., 2016. A Modified P&O Maximum Power Point Tracking Method With Reduced Steady-State Oscillation and Improved Tracking Efficiency. IEEE Transactions on Sustainable Energy 7, 1506–1515. doi:10.1109/TSTE.2016.2568043.

[5] Aourir, M., Abouloifa, A., Lachkar, I., Aouadi, C., Giri, F., Guerrero, J.M., 2020. Nonlinear control and stability analysis of single stage grid-connected photovoltaic systems. International Journal of Electrical Power & Energy Systems 115, 105439. doi:10.1016/j.ijepes.2019.105439.

[6] Biricik, S., 2017. Grid Voltage Sensorless Single-Phase Half-Bridge Active Filter and DC Bus Voltage Regulation. Electric Power Components and Systems 45, 2131–2140. doi:10.1080/15325008.2017.1407839.

[7] Chowdhury, M.A., Kashem, S.B.A., 2018. H_∞ loop-shaping controller design for a grid-connected single-phase photovoltaic system. International Journal of Sustainable Engineering 11, 196–204. doi:10.1080/19397038.2018.1444680.

[8] Echalih, S., Abouloifa, A., Hekss, Z., Lachkar, I., 2019a. Half Wave Control Strategy of Interleaved Buck Converter Based Single Phase Active Power Filter for Power Quality Improvement, in: 2019 4th World Conference on Complex Systems (WCCS), IEEE, Ouarzazate, Morocco. pp. 1–6. doi:10.1109/ICoCS.2019.8930737.

[9] Echalih, S., Abouloifa, A., Lachkar, I., Hekss, Z., Aourir, M., Giri, F., 2019b. Hybrid Control of Single Phase Shunt Active Power Filter Based on Interleaved Buck Converter, in: 2019 American Control Conference (ACC), IEEE, Philadelphia, PA, USA. pp. 3636–3641. doi:10.23919/ACC.2019.8814917.

[10] Fang, Y., Fei, J., 2019. Adaptive Backstepping Current Control of Active Power Filter Using Neural Compensator. Mathematical Problems in Engineering 2019, 1–9. doi:10.1155/2019/5130738.

[11] Fang, Y., Fei, J., Wang, T., 2020. Adaptive Backstepping Fuzzy Neural Controller Based on Fuzzy Sliding Mode of Active Power Filter. IEEE Access 8, 96027–96035. doi:10.1109/ACCESS.2020.2995755.

[12] Fei, J., Chen, Y., 2020. Dynamic Terminal Sliding-Mode Control for Single-Phase Active Power Filter Using New Feedback Recurrent Neural Network. IEEE Trans. Power Electron. 35, 9906–9924. doi:10.1109/TPEL.2020.2974470.

[13] Fei, J., Wang, H., 2019. Experimental Investigation of Recurrent Neural Network Fractional-order Sliding Mode Control of Active Power Filter. IEEE Trans. Circuits Syst. II , 1–1doi:10.1109/TCSII.2019.2953223.

[14] Fei, J., Zhang, S., Zhou, J., 2012. Adaptive Sliding Mode Control of Single-Phase Shunt Active Power Filter. Mathematical Problems in Engineering 2012, 1–22. doi:10.1155/2012/809187.

[15] Giri, F., Abouloifa, A., Lachkar, I., Chaoui, F.Z., 2010. Formal Framework for Nonlinear Control of PWM AC/DC Boost Rectifiers—Controller Design and Average Performance Analysis. IEEE Trans. Contr. Syst. Technol. 18, 323–335. doi:10.1109/TCST.2009.2022014.

[16] Harrag, A., Messalti, S., 2015. Variable step size modified P&O MPPT algorithm using GA-based hybrid offline/online PID controller. Renewable and Sustainable Energy Reviews 49, 1247–1260. doi:10.1016/j.rser.2015.05.003.

[17] Hekss, Z., Abouloifa, A., Echalih, S., Lachkar, I., 2019a. Cascade Nonlinear Control of Photovoltaic System Connected to Single Phase Half Bridge Shunt Active Power Filter, in: 2019 4th World Conference on Complex Systems (WCCS), IEEE, Ouarzazate, Morocco. pp. 1–6. doi:10.1109/ICoCS.2019.8930796.

[18] Hekss, Z., Lachkar, I., Abouloifa, A., Echalih, S., Aourir, M., Giri, F., 2019b. Nonlinear Control Strategy of Single Phase Half Bridge Shunt Active Power Filter Interfacing Renewable Energy Source and Grid, in: 2019 American Control Conference (ACC), IEEE, Philadelphia, PA, USA. pp. 1972–1977. doi:10.23919/ACC.2019.8814428.

[19] Hoon, Y., Mohd Radzi, M., Hassan, M., Mailah, N., 2017. Control Algorithms of Shunt Active Power Filter for Harmonics Mitigation: A Review. Energies 10, 2038. doi:10.3390/en10122038.

[20] Khalil, H., 2002. Nonlinear Systems. Prentice Hall.

[21] Kissaoui, M., Abouloifa, A., Abouelmahjoub, Y., Chaoui, F.Z., Giri, F., 2016. Output-Feedback Nonlinear Adaptive Control of Single-Phase Half-Bridge Ups Systems: Output-Feedback Nonlinear Adaptive Control of Single-Phase Half-Bridge Ups Systems. Asian Journal of Control 18, 1995–2009. doi:10.1002/asjc.1293.

[22] Komurcugil, H., Kukrer, O., 2006. A new control strategy for single-phase shunt active power filters using a Lyapunov function. IEEE Trans. Ind. Electron. 53, 305–312. doi:10.1109/TIE.2005.862218.

[23] Kukrer, O., Komurcugil, H., Guzman, R., De Vicuna, L.G., 2020. A New Control Strategy for Three-Phase Shunt Active Power Filters Based on FIR Prediction. IEEE Trans. Ind. Electron. , 1–1doi:10.1109/TIE.2020.3013761.

[24] Mahanty, R., 2014. Indirect current controlled shunt active power filter for power quality improvement. International Journal of Electrical Power & Energy Systems 62, 441–449. doi:10.1016/j.ijepes.2014.05.002.

[25] Mchaouar, Y., Taghzaoui, C., Abouloifa, A., Fettach, M., Ellali, A., Lachkar, I., Giri, F., 2019. Sensorless Nonlinear Control Strategy of the Single Phase Active Power Filters via Two-time Scale Singular Perturbation Technique. ujeee 6, 383–401. doi:10.13189/ujeee.2019.060509.

[26] Mohd Zainuri, M., Mohd Radzi, M., Che Soh, A., Mariun, N., Abd Rahim, N., Hajighorbani, S., 2016. Fundamental Active Current Adaptive Linear Neural Networks for Photovoltaic Shunt Active Power Filters. Energies 9, 397. doi:10.3390/en9060397.

[27] Ouadi, H., Ait Chihab, A., Giri, F., 2015. Adaptive nonlinear control of three-phase shunt active power filters with magnetic saturation. International Journal of Electrical Power & Energy Systems 69, 104–115. doi:10.1016/j.ijepes.2014.12.089.

[28] Ouchen, S., Betka, A., Abdeddaim, S., Menadi, A., 2016. Fuzzy-predictive direct power control implementation of a grid connected photovoltaic system, associated with an active power filter. Energy Conversion and Management 122, 515–525. doi:10.1016/j.enconman.2016.06.018.

[29] Rahmani, S., Mendalek, N., Al-Haddad, K., 2010. Experimental Design of a Nonlinear Control Technique for Three-Phase Shunt Active Power Filter. IEEE Trans. Ind. Electron. 57, 3364–3375. doi:10.1109/TIE.2009.2038945.

[30] Salimi, M., Soltani, J., Zakipour, A., 2017. Experimental design of the adaptive backstepping control technique for single-phase shunt active power filters. IET Power Electronics 10, 911–918. doi:10.1049/iet-pel.2016.0366.

[31] Vaquero, J., Vázquez, N., Soriano, I., Vázquez, J., 2018. Grid-Connected Photovoltaic System with Active Power Filtering Functionality. International Journal of Photoenergy 2018, 1–9. doi:10.1155/2018/2140797.